University Of Twente

Project Module 8

Project Mechatronics 2020

Design and experimentally verify a mirror manipulator for free space optical (FSO) communication from ground to space

Authors
J.M. van Haastregt s2137844
J.L. Alvarez s2032147
A.E. Mino s2074486
D.R. Gavilanes s2074478
L.A Pérez s2029413
D.S. Chiriboga s2074117

Tutor
K.S. Dwarshuis

November 4, 2021

Contents

1 Concept

1.1 Overview of the Mechatronic System

The system has two wire flexures and one leaf spring to constraint its motion and get one degree of freedom. The two wire flexures are connected to the upper surface of the mirror plate while the leaf spring is connected perpendicular to the bottom surface (see figure 1). The hardware components in this system are: a magnetic encoder, a motor, a microcontroller and an amplifier. The magnetic encoder will follow and record the position of the mirror plate while the motor will move it up and down. Inputs to the system are calculated by the microcontroller. The microcontroller bases its calculations on the position output by the encoder. It sends a PWM to the amplifier, which gives a voltage to the motor. The magnetic encoder will be located next to the motor, attached to a metallic plate which in turn is connected to the mirror plate. This makes the system collocated. The motor will be attached to the mirror plate from below as can be seen in figure 1.

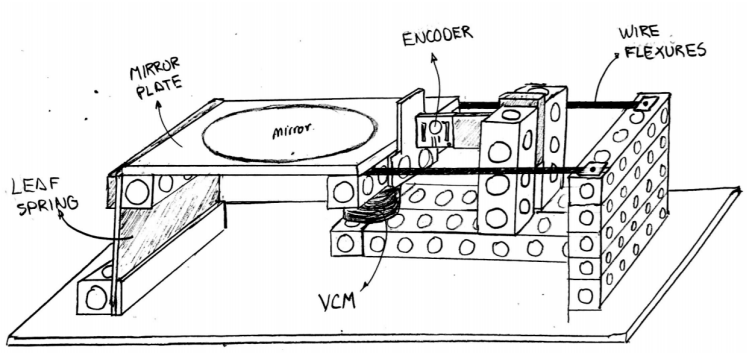

Figure 1: Sketch of Mechatronic System

1.2 Requirements

In the rest of this paper the tracking system will be designed. In order to reach a good result, the system should comply with the requirements listed below.

Functional requirements

- The satellite can be tracked with one degree of freedom.
- The mirror can rotate with a maximum speed of 19.5mrad/s.
- The tracking accuracy is 25 µrad, which amounts to 50 µrad for the laser beam by the law of reflection.
- The maximum angle between stator and rotor is ±17.5 mrad [1]. Taking into account the speed of the satellite, this means that the satellite should be tracked for around two seconds.
- The maximum force the VCM is allowed to output is 4.63N [1]. This is to avoid overheating.
- The system should be stable with a minimum phase margin of 25 degrees.
- The stresses in the wire flexures should not exceed the yield stress of 195MPa [2].
- The voltage output of the amplifier is within -24V and 24V.

Additional requirements

- Higher order dynamics should not get into play.
- The maximum dimensions of the system are 0.5x0.5x0.5m (lxbxh).
- Components should be replaceable easily.
- The system should be stopped when either the voltage, force or position gets outside its boundaries (which could happen in case of an error).

Additional hardware specifications

- The mirror has a diameter of 25.4mm.

- Additional parts can only be created from lasercutting with a thickness of 0.1 to 0.6mm in increments of 1mm.
- A C2000 microcontroller is used.
- A linear sensor is used with 8192 counts per 2mm.
- The laser has a wavelength of 1550nm.

1.3 Kinematic Structure

The design consists of one leaf spring and two wire flexures connected to the rigid body that support the mirror, as can be seen in figure 2. The structure is meant to constrain five DOFs leaving one rotation out to move the mirror. The remaining rotation is around the Z-axis where the constraints intersect. This will be actuated by the VCM connected directly to the opposite edge of the mirror.

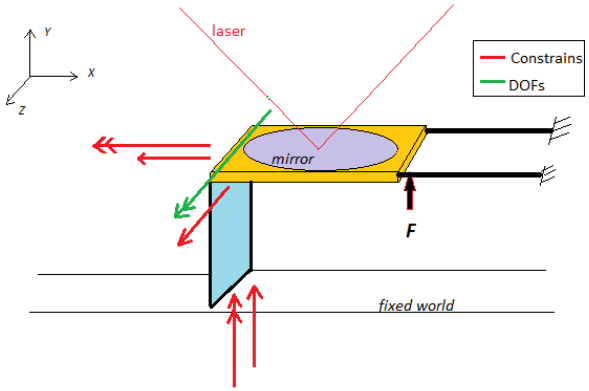

Figure 2: Kinematic structure

1.4 Nominal Dynamics

1.4.1 1DOF system and its frequency response

The dynamic analysis of the mechanism was started by means of a simple model which will be used for the continuing of the report. The simple model is showed in figure 3:

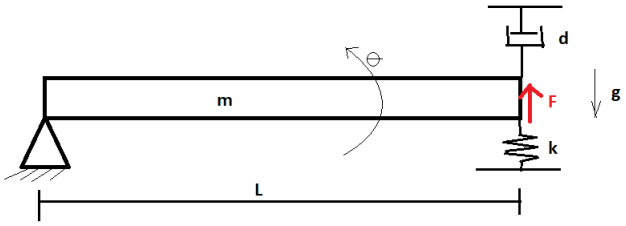

Figure 3: Simple model 1DOF

From a kinematic analysis it followed that there is one point mass ($Nb = 1$) and three generalized coordinates ($Nq = 3$, x,y and θ). Furthermore, there is one constrain on x-displacement, and a constant length so $Nc = 2$. This results in one degree of freedom. The displacement in Y-direction is what will be measured by the sensor, so $q_i = Y$ and $q_d = \theta$. Since the rotation of the mirror is with a small angle of 35 mrad the approximation $sin\theta = \theta$ is used.

$$\theta = y/L \longrightarrow \dot{\theta} = \dot{y}/L \tag{1}$$

The equations of motion are determined using Lagrange's method:

$$\frac{d}{dt}(\frac{\partial T}{\partial \dot{q}_i}) - \frac{\partial T}{\partial q_i} + \frac{\partial V}{\partial q_i} + \frac{\partial D}{\partial \dot{q}_i} = Q_i \tag{2}$$

$$I = \frac{1}{3}m(b^2 + L^2) \tag{3}$$

At the end the equation of motion with linearization is the following:

$$(\frac{b^2 + L^2}{L^2})\frac{m}{3}\ddot{y} + d\dot{y} + ky = F \tag{4}$$

By rewriting the equation in terms of a standard single degree of freedom system, the natural frequency and damping factor are derived.

$$\omega_n = \sqrt{\frac{3kL^2}{(b^2 + L^2)m}}, \qquad \zeta = \frac{3L^2 d}{2\omega_n(b^2 + L^2)m} \tag{5}$$

Finally, the maximum equivalent stiffness of the wire flexures that can be used is calculated with the nominal force of the motor and a desired vertical displacement of $\theta \cdot L$ assumed with an arm of 40mm.

$$k = F/\theta L = 2.97N/mm \tag{6}$$

1.4.2 Electrical subsystem

The model of the electrical subsystem can be seen in figure 4. It consists of four parts, a voltage input U(t) which is provided for the PWM voltage amplifier, an electrical resistance of the motor (Re), a self-inductance (Lc) and the motor constant (km). The actuator is a voice coil motor which provide a linear force.

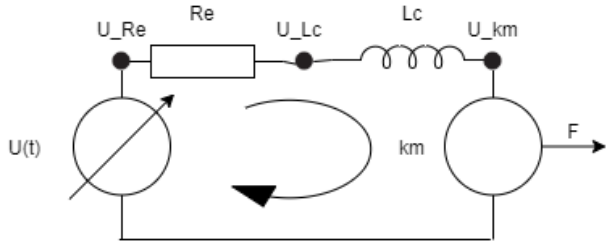

Figure 4: Electric circuit model of the motor

Equations for resistance, self-induced coil and the sum of the voltages are as follows.

$$I = \frac{1}{Lc}\int U_{Lc}dt, \qquad U_{Re} = I * Re, \qquad U_{Lc} = U(t) - km * v - I * Re \tag{7}$$

Taking the electrical model and the previous equations a block diagram was derived. The block diagram can be seen below in Fig.5a, this has two inputs, one is the voltage U(t) and the other is the velocity that comes from the mechanical model in Fig.5b.

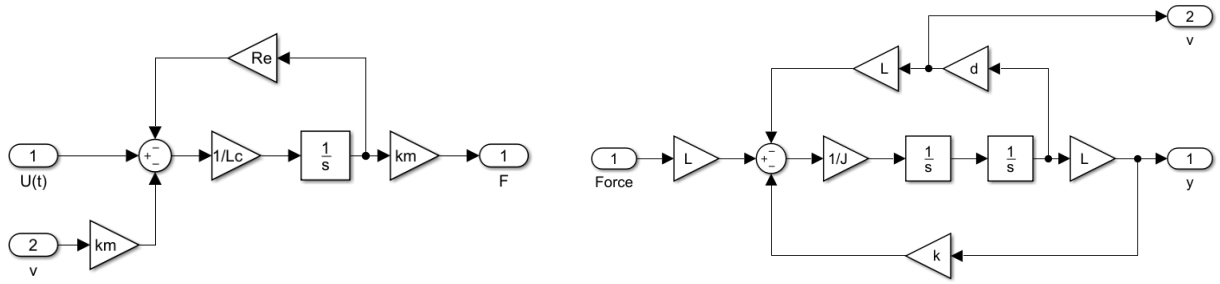

(a) Block diagram of electric part

(b) Block diagram of mechanical part

Figure 5: Block Diagrams

1.5 Controller Design

The system needs a controller. There is a need for P-action to reduce the sensitivity to disturbances and D-action to add damping. Furthermore, the input is Linear. Therefore, there is a need for I action to raise the system type. Otherwise, there would be an infinite error. With this knowledge, it is chosen to use a PID controller. Finally, feed-forward is used to keep the crossover frequency low. This way, no higher order dynamics will get into play.

Using the requirement for the maximum servo-error, the properties of the controller can be calculated using formula 8[3]. Using the reference trajectory the instance with the highest error was found. Via this instance, ω_c could be calculated.

$$e_{LF} = \frac{\beta}{\alpha \cdot \omega_c^3} \cdot ((1-\gamma)\dddot{r}(t) + (1-\gamma)2\zeta\omega_1\ddot{r}(t) + (1-\gamma)\omega_1^2\dot{r}(t)) \tag{8}$$

The following parameters are used:

- α and β are estimated to be 0.2 and 2 respectively. In the analysis later on it will be found if these values are the most optimal.
- e_{max} is $25\mu rad$ because this is the required maximum servo error
- γ is taken as 0.9, for a 90% certainty on the system properties.

With the found crossover frequency of 277 rad/s, the values for the PID controller can be found according to equations 9[4].

$$\tau_z = \frac{\sqrt{\frac{1}{\alpha}}}{\omega_c} = 0.0081, \qquad \tau_i = \beta \cdot \tau_z = 0.0162, \qquad \tau_p = \frac{1}{\sqrt{\frac{1}{\alpha}} \cdot \omega_c} = 0.0016, \qquad k_p = \frac{m_{eq} \cdot \omega_c^2}{\sqrt{\frac{1}{\alpha}}} = 893.9 \tag{9}$$

Where the value for m_{eq} is given by eq.10 [5], in which k_T is equal to the back EMF (7.35 V/(m/s)), R is the resistance 10.22 and m = 0.06 kg. This mass is taken higher than the mirror mass, in order to keep the crossover frequency low. This can be achieved in reality by adding mass to the mirror plate.

$$m_{eq} = \frac{m}{\frac{k_T}{\sqrt{R}}} = 0.026 \ \ [kg] \tag{10}$$

This controller results in the bode plot as shown in figure 6. Using the bode plot, the margins can be found: GM = ∞, PM = 31.

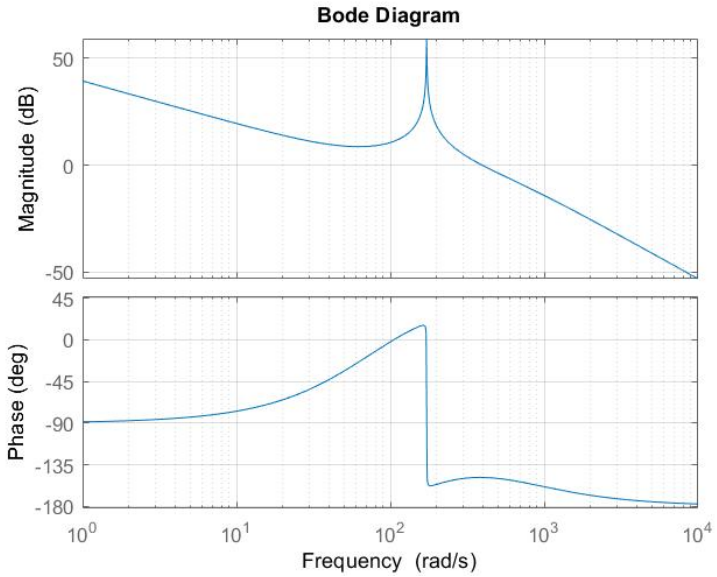

Figure 6: Bode Plot of the Plant + PID Controller

2 Design

In chapter 1, some dimensions of the different components were assumed in order to get a stiffness. For the spacar model, these measurements were used to create a model but, a very high resulting stress, higher than the yielding stress of the material, was found in order to reach the required motion. After a trial and error process an equilibrium was found and the dimensions of the elastic guidance components were obtained and are listed in table 1.

Parameter	Description	Value	Parameter	Description	Value
ρ	Density	7900 kg/m^3	L_{leaf}	Length of leaf spring	30 mm
E	Young's Modulus	200 MPa	b_{leaf}	Width of leaf spring	40 mm
G	Shear Modulus	76 MPa	t_{leaf}	Thickness of leaf spring	0.2 mm
L_{mirror}	Length of mirror plate	40 mm	L_{wire}	Length wire flexure	60 mm
b_{mirror}	Width of mirror plate	40 mm	b_{wire}	Width wire flexure	2.2 mm
t_{mirror}	Thickness of mirror plate	0.3 mm	t_{wire}	Thickness wire flexure	0.2 mm

Table 1: Dimensions

With these dimensions of the system, a 3D CAD model is presented in figure 7.

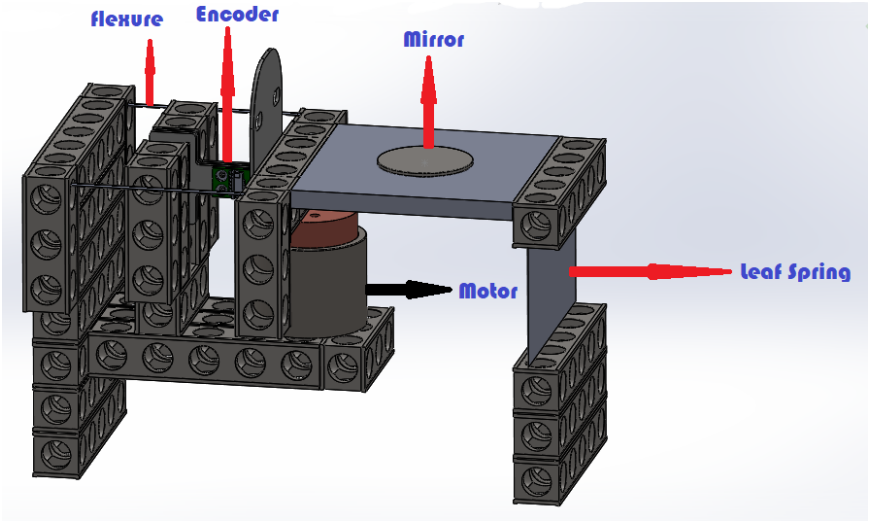

Figure 7: CAD Model of the Mechatronic System

With this dimensions, an analysis of the important parameters of the system was made to prove the correct performance of the model. In figure 8 all the forces and reactions are shown for which the analysis was made and also the stress formula for a deflecting beam under load.

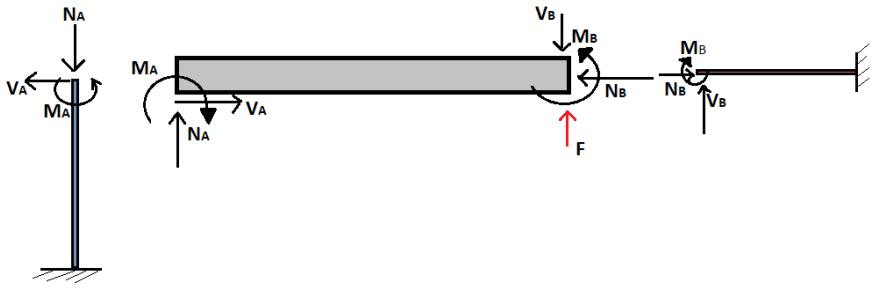

Figure 8: FBD of mirror model.

$$\sigma = \frac{My}{I} \tag{11}$$

after the computation of forces based on the model on fig. 8 the terms should be replaced by the following

$$M = \frac{EI\theta}{L}, \qquad y = \frac{t}{2} \tag{12}$$

which result on the following equation for the maximum stress

$$\sigma = \frac{E\theta t}{2L} \tag{13}$$

Where $\theta = 35mrad$, t is the thickness and L the length depending on the measures given above for each element. After calculation the results are presented in Table 2 where only the maximum stress is included which resulted to be at the wire flexures elements.

Parameter	Description	Value
$F_{deflection}$	Force at deflection	0.368 N
u_{leaf}	Deflection of leaf flexure	0.59 mm
u_{wire}	Deflection of wire flexures	1.17 mm
σ_{max}	Max. Stress	26 MPa

Table 2: Resultant values

2.1 Extended Dynamic Model

Using spacar, the system was modelled and analysed in order to get a list of the eigenfrequencies and the most relevant modes.

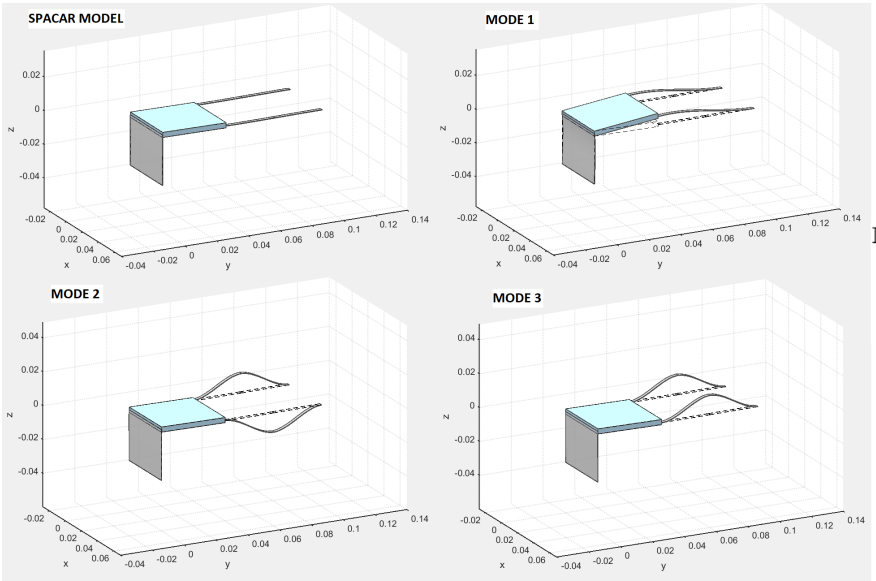

Mode	Frequency
1	196.03 rad/s
2	1782.5 rad/s
3	1793.5 rad/s

Figure 9: Relevant modes of system

In figure 9 it is shown the relevant modes with their respective frequencies up until the Nyquist frequency which reduces the range of importance. In that case, Mode 1 is the desired response for the system and the 2 remaining modes are the parasitic modes which effect is reduced by tuning the control and discretization explained in the following chapters.
The frequency response is shown in figure 10 for the electromechanical system.

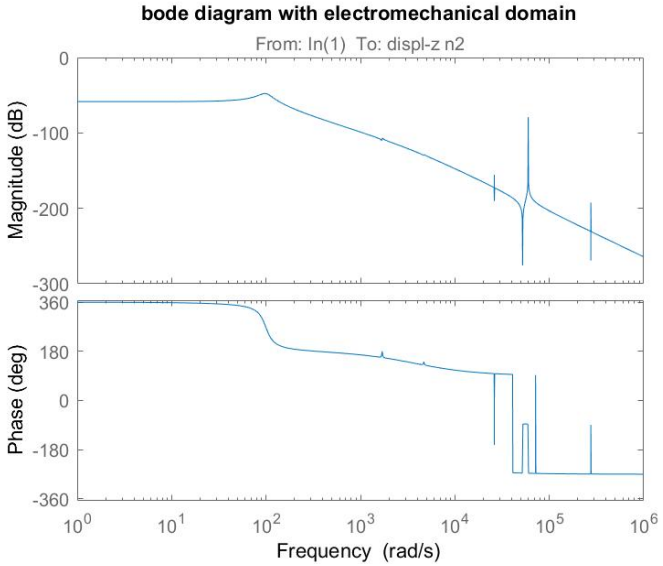

Figure 10: Frequency response for the electromechanical system

2.2 Effects of parasitic frequencies, discretisation and computation delay

Using the spacar model, it can be found that the parasitic frequencies have effects on the bode plot and moreover, an effect on the stability of the system. One reason is that the parasitic frequencies reduce the phase. Where first the phase did not cross -180 degrees, now this is the case and thus the gain margin is not infinite anymore. Another effect of the parasitic frequencies is that there are peaks that cross the 0 dB gain. However, these peaks are after the nyquist frequency so they do not have to be removed by the controller.

The discretisation also has an effect on the bode plot and especially on the stability margins. The controller has been discretised using Tustin's method, as this is the more precise for the phase, see figure 11. However, the biggest change is in the discretisation of the plant. The phase decreases drastically near the nyquist frequency, making the gain margin smaller.

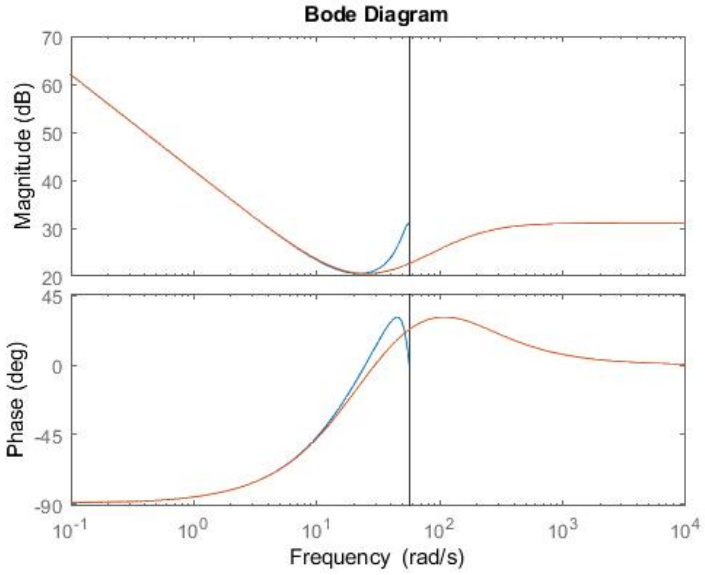

Figure 11: Discrete PID controller using the Tustin's method

Lastly, the factor that is most challenging is the delay that is implemented between the controller and the plant, to account for computation time. This delay decreases the phase with a considerable amount, making the phase margin just a couple degrees, which is unfavourable.

The following changes should be made to the controller or plant to improve the system. Other parameters have been kept the same since they were already in an optimal form.

- α is reduced to 0.1. This increases the phase margin without increasing the cross-over frequency to much.
- β is increased to 4. This increases the phase margin further without increasing the cross-over frequency to much.
- The length of the mirror plate is increased to 60mm, so that the inertia is increased. This leads to the crossover frequency decreasing and parasitic frequencies not interfering anymore.
- γ has been reduced to 0.7. This is because the system is not known as precisely as initially thought.

With the new parameters the margins have been increased from GM = 5.53dB, PM = 7.14 to GM = 14.3dB, PM = 30.2 (see figure 12).

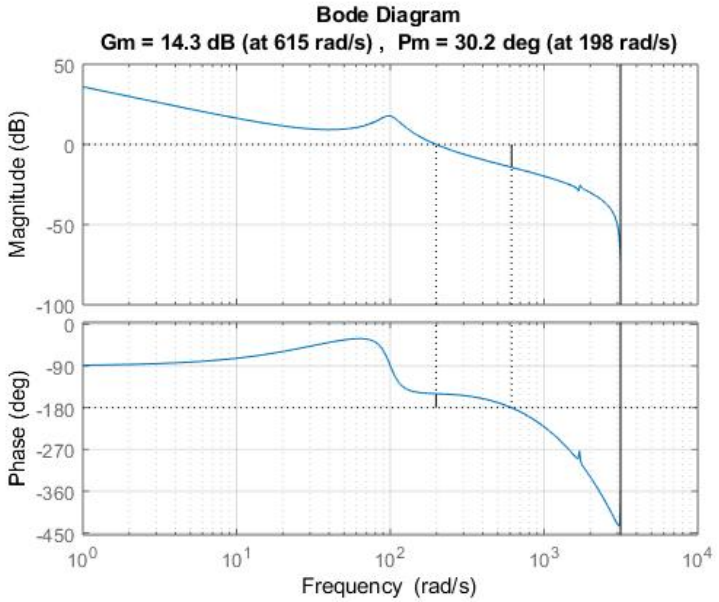

Figure 12: Final bode diagram: Electro-mechanical system with Controller

To double check the stability of the system, the nyquist diagram of the discretised system is plotted in figure 13. Using zpkdata in MatLab it is found that there are no pools in the discretised system with an absolute value greater than 1. Also, there are no encirclements of -1 in the nyquist plot. This means that the system is indeed stable.

2.3 Limitations and trade-offs

Several factors have an influence on the performance and stability of the system.

For the controller, the specifications that can be tuned are α and β. Previously, it has been discovered that the phase margin had to be increased. The phase margin can be increased by decreasing α and by increasing β. However, when decreasing α too much, the high frequency gain increases also resulting in the cross-over frequency to increase. Also when increasing β too much the cross-over frequency increases.

For the plant, the inertia and stiffness are the most important specifications, which can be tuned by changing the dimensions. The damping can not be tuned easily, therefore this will be left out of consideration. First

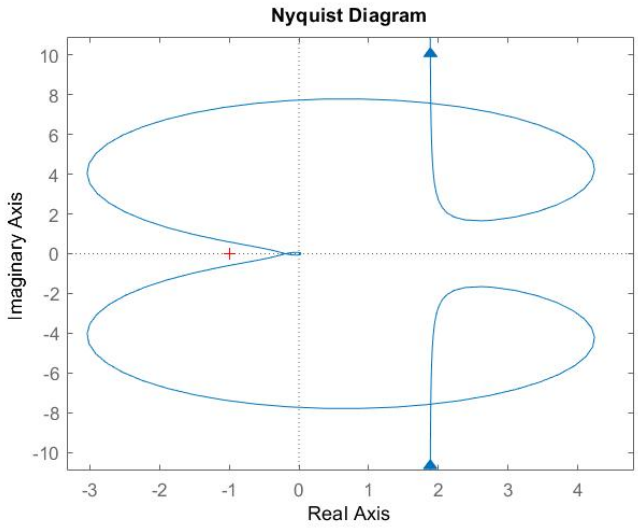

Figure 13: Nyquist diagram of the controler and electromechanical system

off, the inertia should be high enough relative to the stiffness. If this would not be the case, the natural frequency would be high, resulting in a high cross-over frequency and higher order behaviour interfering. Furthermore, if this is not the case the low frequency approximations made for the controller do not hold and there will be too much of a discrepancy between the controller and the actual output. However, the inertia should not be too high, since the actuator needs to be able to accelerate the system well enough. Moreover, the maximum stress in the flexures will get too high if the inertia is to big, since a bigger force will be applied. Also, the stiffness should also not be too low since this will make the system unstable and parasitic frequencies will decrease, and thus interfere.

The stiffness of the flexures can be tuned with the thickness and the length. The thickness should be small enough to keep the stiffness low, but not too small so that the stresses get too high. For the length, it should be large enough so that the stiffness stays low, but not be too long to keep the stresses low enough also.

3 Implementation

3.1 Modelling in simulink

To verify the design and Performance, a simulink model is necessary. The simulink model is set up in a way that it represents the real-life setup and hardware as closely as possible.

As input for the model a reference trajectory for the mirror is used. This reference trajectory consists of a function for position, velocity and acceleration.

Both the controller and the plant have been modelled in the linear domain. This means that the input to the controller is in meters and the output is a force. For the plant the input is a voltage and the output in meters. The feedforward has a force as output like the controller. In between the controller, conversions have been added to stay close to reality. This means the controller output is converted to PWM, then converted to a continuous domain before it is converted to a Voltage. The output of the plant is converted to encoder counts, discretised and then converted to radians to compute the error. Finally, the output of the controller is limited to the maximum continuous force to avoid overheating of the actuator when an error would occur.

The full block diagram of the simulink model is given in figure 14. The controller is a simple block diagram of the PID split in P-, D-, and I-action, combined with a lead filter. At the integrator, the output is limited to avoid integrator windup.

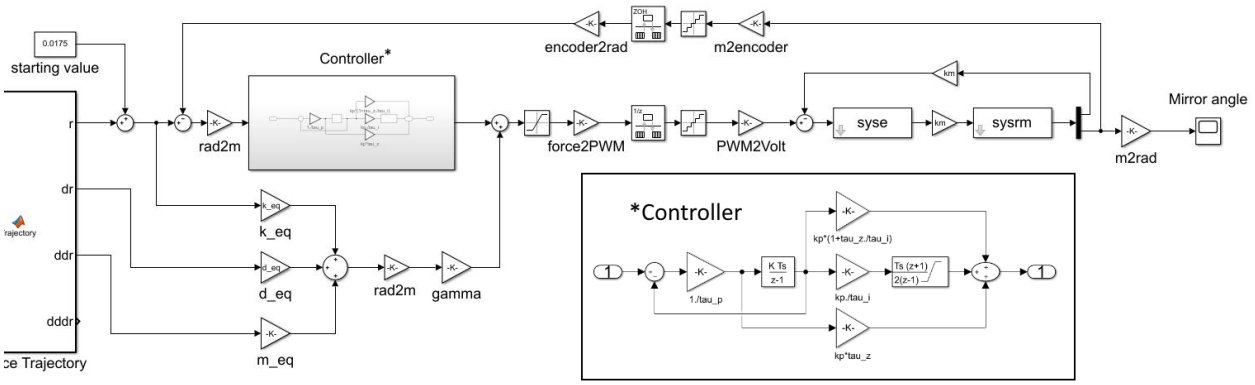

Figure 14: Block diagram of the simulink model

3.2 Results of Simulations

3.2.1 Static Gain

To check the static gain with the simulation, the modeled static gain is obtained from the end value theorem where $k = 1/G(0)$ [4].

$$lim_{s\to 0} G(s) = 1/k = \frac{1.748 \times 10^{151}}{1.476 \times 10^{154}} = 0.0012 \tag{14}$$

In figure 15 it can be observed that the the graph converges to this value when the simulation time is the time before the error is within 1% which is obtained with [4]:

$$t = \frac{ln(0.01)}{-\zeta \times W_n} = 0.42s \tag{15}$$

3.2.2 Linearity

In figure 15 the linearity of the electromechanical system is shown. A step input was applied to the transfer function of the plant. To check its linearity it was proved that if the input is doubled then the output must result doubled as well. To prove it in a better way, a static gain of 0.5 was applied after the system to check if both lines overlap.

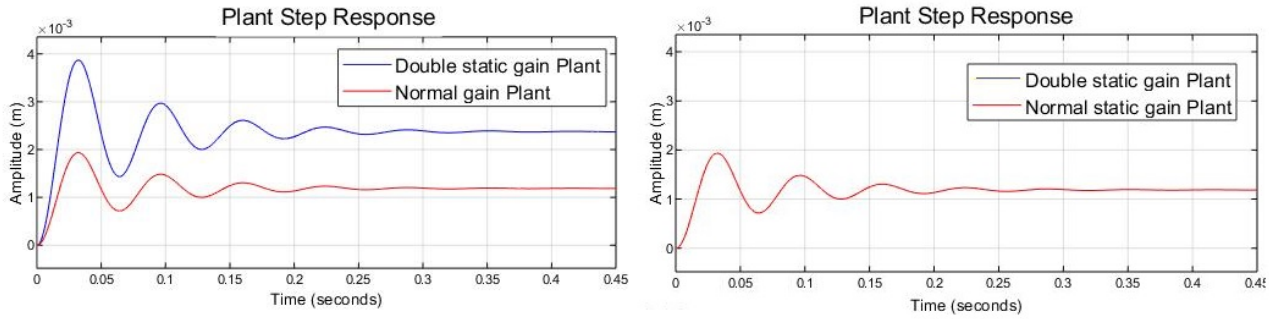

Figure 15: Left) The red line is the step response of the electromechanical system. The blue line is the step response with a doubled input. Right) An overlap is seen when a static gain of 0.5 is applied to check its linearity.

3.2.3 Frequency response and Linearity

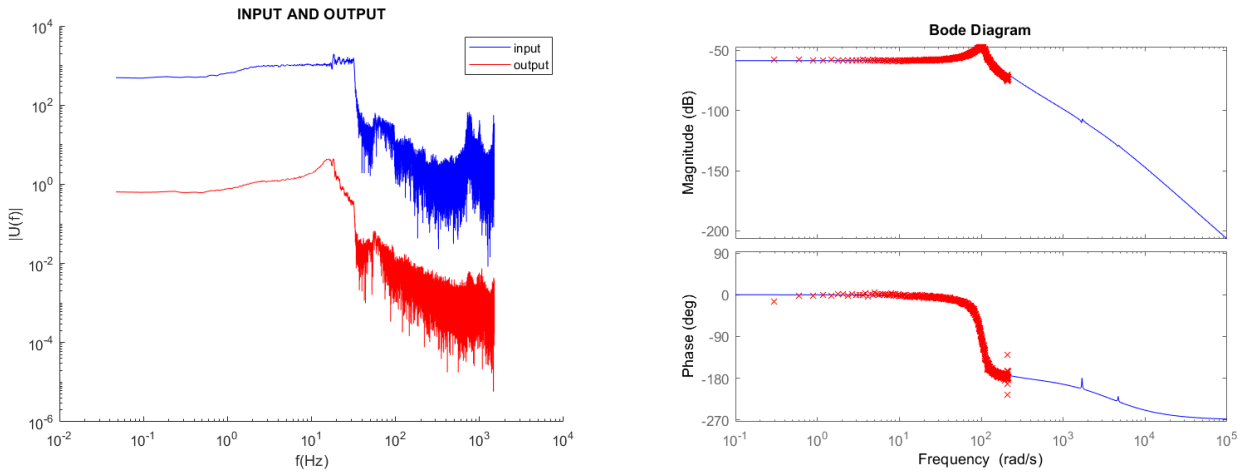

Figure 16: Frequency Response FRF

The system designed should have a linear behaviour and for checking that a possible approach is to select 2 input signals and test them in the simulink model measuring the output. One of the signals has to be multiplied with a random constant and if the system behaves linearly the output of the first signal should be equal to the second signal times the constant that we choose.

To verify that the model implemented in this project was designed properly we need to check if the frequency response matches the results from the SPACAR model. In the right plot of figure 16 it can be clearly seen that the frequency response of the system together with the controler matches the frequency response of the real system modeled in SPACAR. It can be proved that at low frequencies the output of the system follows the same path as the desired response. This occurs only before the 200 rad/s frequency, as we are interested on the first excited frequency which is around 100 rad/s, this does not affect the required performance.

3.3 Performance Verification

Using the simulink model, the requirements set in Chapter 1.2 can be checked. First off, the tracking accuracy is checked. In figure 17 the tracking of the mirror is shown compared to the maximum error stated in the requirements. As can be seen the error is below the maximum error during the whole duration of constant velocity. This means that the purpose of the system, transmitting data to satellites, is fulfilled.

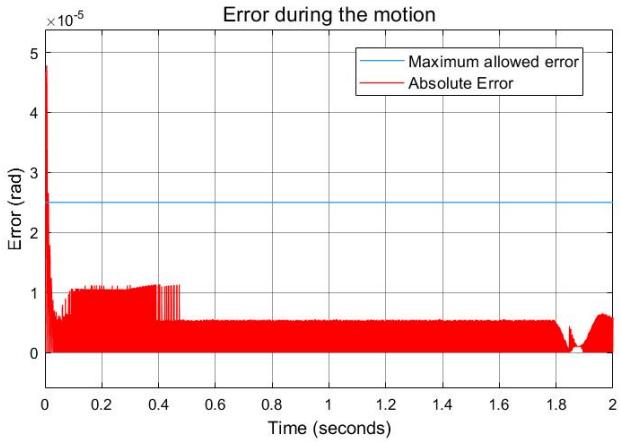

Figure 17: Tracking error of the mirror

Furthermore, in figure 18a, the force output of the actuator is shown. This force is well within limits of the 4.63N continuous force that the motor can output without overheating. In figure 18b, the voltage output is shown. Also here, it can be seen that the voltage stays within the limits of ±24 Volts that the amplifier can output.

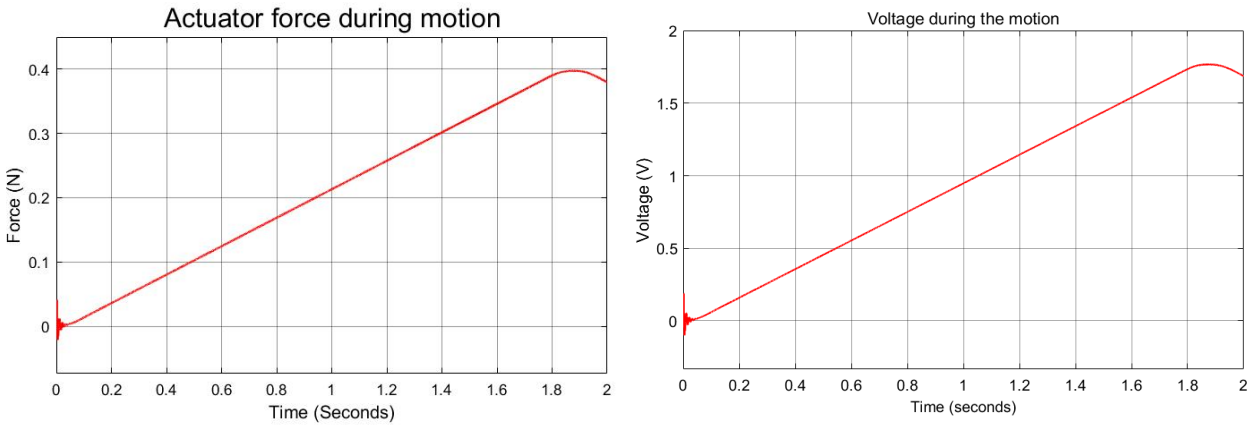

(a) (b)

Figure 18: The actuator force and amplifier voltage outputs

The other requirements, such as the phase margin and maximum stresses, are also fulfilled. This has been described in previous chapters.

4 Conclusions and recommendations

It can be concluded from the verifications that the system has a sufficient performance. It fulfills all the requirements. However, there are of course still improvements that can be made.

One improvement could be to use a smaller motor, since the forces needed are quite a lot smaller than the maximum continuous force of the motor that is currently used.

Furthermore, values for the controller could be tuned even more thoroughly to get a smaller maximum error than set in the requirements. Although, since the laser beam will be diverging, a more precise system will not make that big of a difference in fulfilling its function.

Something that is not considered in this report, but could be taken a look at is the suppression of vibrations from the ground. Since this system needs to be very accurate, external vibrations should not be allowed to interfere.

Finally, it is recommended to still check the robust stability of the system. Even though the system has been verified to be stable, there is always an uncertainty with the model that has been made. Using robust stability it can be assured that deviations in equivalent masses, spring constants, or electrical dynamics of e.g. the encoder will not make the system unstable. If it would follow from this check that the system is not robust, it should be considered to lower the sensitivity, cross-over frequency or to add more damping to the system in order to achieve robust stability. A lower sensitivity can most easily be achieved by reducing the mass.

References

[1] Akribis-Systems, "datasheet avm30-15."

[2] "datasheet provided by university of twente."

[3] W. Hakvoort, "Slides of concept phase provided by university of twente," 2020.

[4] J. van Dijk, R G K M Aarts , G R B E Romer, "Design and control of mechatronic systems," 2019.

[5] D. Collings, "FAQ: What's the difference between torque constant, back EMF constant, and motor constant?," 2017.